Avoiding AC/DC Grid Interaction In MMC Based MTDC Systems

Atsede Gualu Endegnanew
Gilbert Bergna-Diaz
Kjetil Uhlen
Department of Electric Power Engineering
NTNU
Trondheim, Norway

***Abstract*—In this paper, the interaction between ac and dc grids is studied for two types of MMC control structures; conventional and non-conventional control structures. Linear analysis methods that are based mode shapes and participation factors are used to identify dynamic interaction in a hybrid ac-dc power system. The analysis uses as a test system a three terminal Modular Multilevel Converter (MMC) based Multi-terminal High Voltage DC (MTDC) grid connecting three multi-machine asynchronous ac grids. The results show that there is some dynamic interaction between ac and dc grids under conventional MMC converter control structure, while the non-conventional MMC converter control structure decouples the ac and dc side of the MMC converter, thus avoiding interaction between the ac and dc grids.**

***Index Terms*—dc grids; hybrid ac/dc systems; MMC-MTDC; Small signal stability**

I. INTRODUCTION

Interest in multi-terminal high voltage dc (MTDC) grids has grown due to large-scale integration of renewable energy sources in the power system and need for an increased transmission capacity that is driven by power markets. In the future, the MTDC grids will interconnect and operate in parallel with ac system. Therefore, it is of interest to study the dynamics of the entire hybrid ac/dc power system.

AC power dynamics are well studied and understood, while MTDC grid dynamic studies are still an on-going research topic. In particular, recent efforts have been oriented towards obtaining small-signal state-space representation of the Modular Multilevel Converter (MMC), as it is emerging as the most suitable converter topology for Voltage Source Converter (VSC) -based dc Transmission schemes [1]. The methods proposed in [2-5] model the MMC by representing the internal average dynamics of the converter in full detail, by means of several synchronously rotating reference frames. Nonetheless, since the present work is oriented at large-power system studies, where the macroscopic behavior of the converter is favored over a detailed representation of all its internal dynamics, a simplified small-signal model of the MMC is preferred. More precisely, the work is based on the approach presented in [6, 7], where only the aggregated dynamics of the zero sequence circulating current (or the dc current) and the total energy stored in the capacitors of the MMC are modelled, besides the dynamics of the ac-side active and reactive currents. It was shown in [6], that if the modulation indices for the MMC arms are calculated to compensate for the voltage oscillations in the internal equivalent arm capacitor voltages, this approach results in an accurate representation of the ac- and dc-side terminal behavior, while limiting the need for representing the internal variables. Furthermore, it will be shown that these underlying assumptions on the control of the converter can be potentially useful to avoid ac/dc interactions in MTDC systems.

In this paper, a test hybrid ac/dc power system with detailed model of generators, MMC converters and dc cables is used to study dynamic interactions between ac and dc grids. It considers two types of MMC converter control structures, and compares interaction between ac grid and MTDC converters, and interaction between asynchronous ac grids under the two converter control structures. Linear analysis methods, which are based mode shapes and participation factors for the analysis, are used in the study. The results show that there is some dynamic interaction between ac and dc grids for one type of converter control structure while the other type of control decouples the ac and dc grid dynamics.

II. HYBRID AC/DC GRID MODELLING

A. Generator and ac network model

A sixth-order model [8], which represents the synchronous generators as subtransient *emfs* behind subtransient reactances, is used to model the dynamic behavior of all generators. The differential equations for each synchronous generator *i* are:

$$
\begin{aligned}
\dot{\delta}_i &= \omega_0\left(\omega_i - \omega_s\right) = \omega_0 \Delta\omega_i \\
\dot{\Delta\omega}_i &= \frac{1}{2H_i}\left(P_{mi} - P_{ei} - D_i\Delta\omega_i\right) \\
\dot{E}'_{qi} &= \frac{1}{T'_{d0i}}\left(E_{fdi} - E'_{qi} + I_{di}\left(x_{di} - x'_{di}\right)\right) \\
\dot{E}'_{di} &= \frac{1}{T'_{q0i}}\left(-E'_{di} - I_{di}\left(x_{qi} - x'_{qi}\right)\right) \\
\dot{E}''_{qi} &= \frac{1}{T''_{d0i}}\left(E'_{qi} - E''_{qi} + I_{di}\left(x'_{di} - x''_{di}\right)\right) \\
\dot{E}''_{di} &= \frac{1}{T''_{q0i}}\left(E'_{di} - E''_{di} - I_{qi}\left(x'_{qi} - x''_{qi}\right)\right)
\end{aligned}
\tag{1}
$$

where δ_i is the angle, in radians, between each machine's rotor q-axis and the reference machine's rotor q-axis, ω_i is rotor speed, $\Delta\omega_i$ is the speed deviation, E'_i and E''_i are transient and sub-transient voltages while x, x' and x'' are synchronous, transient and sub-transient reactances, respectively. H_i is inertia constant in seconds, while T_0' and T_0'' are the open-circuit transient and sub-transient time constants, respectively. Furthermore, ω_0 is the base rotor speed in rad/s and ω_s is the synchronous speed, which is the speed of the reference machine.

The excitation system for all generators is modeled as simple excitation system (SEXS) type of automatic voltage regulator (AVR). The governing equations for an AVR model connected to generator i are:

$$
\begin{aligned}
\dot{E}_{fdi} &= \frac{1}{T_{Ei}}\left(K_i x_{AVRi}\left(1 - \frac{T_{Ai}}{T_{Bi}}\right) + \frac{K_i T_{Ai}}{T_{Bi}}\left(V_{refi} - V_{ti}\right) - E_{fdi}\right) \\
\dot{x}_{AVRi} &= \frac{1}{T_{Bi}}\left(V_{refi} - V_{ti} - x_{AVRi}\right)
\end{aligned}
\tag{2}
$$

where T_{Ai} and T_{Bi} are lead-lag controller time constants, K_i is the controller gain parameter, T_{Ei} is the exciter time constant, E_{fdi} is field voltage and x_{AVRi} a state variable associated with the lead-lag controller. The AVR takes in the reference voltage (V_{ref}) and the generator's terminal voltage (V_t) as an input.

In addition, the ac grid model includes governor system for system frequency regulation. TGOV1 type of turbine and governor model was used in some of the generators. The governing equations for the TGOV1 connected to generator i are:

$$
\begin{aligned}
\dot{x}_{GOV1i} &= \frac{1}{T_{1i}}\left(\frac{1}{R_i}\left(\omega_i - \omega_{refi}\right) - x_{GOV1i}\right) \\
\dot{x}_{GOV2i} &= \frac{1}{T_{3i}}\left(x_{GOV1i} - x_{GOV2i}\right) \\
P_{mi} &= x_{GOV1i} + \left(x_{GOV1i} - x_{GOV2i}\right)\left(\frac{T_{2i} - T_{3i}}{T_{3i}}\right) - D_{ti}\omega_i
\end{aligned}
\tag{3}
$$

where T_{1i} is governor time constant, T_{2i} and T_{3i} are heater time constants, ω_i and ω_{refi} are measured and reference speeds, respectively. D_t is the turbine damping constant, while R is the frequency droop parameter of the turbine.

The ac network representation considers generators and converters as voltage sources behind the appropriate impedances. For load flow calculations, the series connected voltage sources and impedances are converted to Norton equivalent current sources with parallel impedances. These parallel impendences, at generator and converter buses, are augmented to the grid admittance matrix forming $\mathbf{Y_{Aug}}$ to solve the overall network load flow according to (4).

$$
\mathbf{I} = \mathbf{Y}_{Aug}\mathbf{V} \tag{4}
$$

where $\mathbf{I}$ is generators' and converters' current injection vector, and $\mathbf{V}$ is ac bus voltage vector.

B. MMC Converters and their controllers

1) Assumptions on the modelling of the converters

The MMC converter has been modelled in accordance with the approach presented in [6]. Fig. 1. shows an overview of the MMC simplified modelling configuration under two different control structures for a single terminal. This simplified MMC model has been shown to accurately capture the behavior of its terminal ac and dc macroscopic variables (dc and ac voltages and currents). It is also expected to be useful for large power system oriented studies, where the macroscopic behavior is more important than the converter internal dynamics. Nonetheless, it was also shown in [6] that its accuracy is based on some underlying assumptions, recalled here for convenience.

The simplified MMC model under consideration is based on the assumption that the upper and lower insertion indexes are calculated as in (5); i.e., the output of both current controllers e_v^* and u_c^* are divided by the measured sum capacitor voltages of the upper and lower arm of the MMC v_u^{Σ} and v_l^{Σ}.

$$
n_u^{abc} = \frac{-e_v^{*,abc} + u_c^{*,abc}}{v_u^{abc,\Sigma}}, \; n_l^{abc} = \frac{e_v^{*,abc} + u_c^{*,abc}}{v_l^{abc,\Sigma}} \tag{5}
$$

When the insertion indexes are calculated as in (5) the voltages driving the ac-grid and circulating currents e_i and u_c become approximately equal to their reference values. Equation (5) significantly decouples the zero-sequence

dynamics of the energy-sum from the individual energy difference oscillations w_{Δ} [6]. Furthermore, the effect of the *dq*-components of u_c in the energy-sum zero-sequence dynamics can be neglected, as they are significantly smaller than the zero-sequence component u_{cz} [6].

2) Physcial model of the simplifed MMC

From these assumptions, a simplified representation of the MMC is obtained by modelling only the zero-sequence dynamics of the energy-sum w_{Σ}, and the circulating current i_{cz}, as in (6)-(7). In (6), c_{eq} is the total equivalent capacitance per arm of the MMC (i.e. C_{sm}/N with C_{sm} the submodule capacitance), represented in the ac-side per-unit system.

$$\frac{dw_{\Sigma}}{dt} = \frac{\omega_b}{8c_{eq}}\left(\underbrace{-e_{v,d}\cdot i_{v,d} - e_{v,q}\cdot i_{v,q}}_{-p_{ac}} + \underbrace{4u_{c,z}\cdot i_{c,z}}_{p_{dc}} \right) \tag{6}$$

$$\frac{di_{c,z}}{dt} = \frac{\omega_b}{l_a}v_{dc} - \frac{\omega_b}{l_a}u_{c,z} - \frac{r_a\omega_b}{l_a}i_{c,z} \tag{7}$$

The ac-grid current dynamics are expressed as in (8), where ω_g and ω_b are per unit and base grid frequencies, respectively, while r_v and l_v are the sum of filter and half of the arm impedances.

$$\begin{aligned} \dot{i}_{conv,d} &= \frac{\omega_b}{l_v}\left(e^*_{v,d} - v_{pcc,d} - r_v i_{conv,d} + \omega_g l_v i_{conv,q} \right) \\ \dot{i}_{conv,q} &= \frac{\omega_b}{l_v}\left(e^*_{v,q} - v_{pcc,q} - r_v i_{conv,q} - \omega_g l_v i_{conv,d} \right) \end{aligned} \tag{8}$$

The dc voltage dynamics of the cable capacitance connected in between the dc terminals of the MMC is given by (9), where c_{dc} is the border capacitance of the cable model. Furthermore, i_L is the cable current, as defined (17). Note that the zero-sequence of the circulating current is being multiplied by 4 instead of 3 since it is referred to the ac-side per unit system.

$$\dot{v}_{dc} = \frac{\omega_b}{c_{dc}}\left(i_L - 4i_{c,z} \right) \tag{9}$$

3) Outer loop controllers

Two different control schemes for the MMC are investigated in this work, which are depicted in Fig. 1. More precisely, Fig. 1. (a) shows how the active current of the ac grid is being used to regulate the ac-side active power with dc voltage droop control. In addition, the circulating current of the converter is used to regulate the capacitive energy stored in the MMC to a desired reference. For the sake of compactness, this strategy will be referred in this work as the *conventional control*. Conversely, the control structure shown in Fig. 1. (b), hereinafter referred to as *non-conventional control*, uses instead the active ac current to regulate the energy of stored in the MMC to its desired reference. By contrast, the circulating current is used to regulate the power at the dc terminals of the converter with dc voltage droop control and contributes to the dc voltage regulation of the MTDC system.

a) Conventional control

The outer controller regulates ac active power by means of a droop characteristic as well as the reactive power. The outer power-regulating control loop is given in (10), where ρ_d and ρ_q are the states created by the integral part of the PI regulator. In addition, $k_{p,pac}$ and $k_{i,pac}$ are the proportional and integral tuning parameters of the controller.

$$\begin{aligned} i^*_{conv,d} &= k_{p,pac}(p^*_{ac} - p_{ac}) + k_{i,pac}\rho_d \\ \dot{\rho}_d &= p^*_{ac} - p_{ac} \\ i^*_{conv,q} &= k_{p,pac}(q^*_{ac} - q_{ac}) + k_{i,pac}\rho_q \\ \dot{\rho}_q &= q^*_{ac} - q_{ac} \end{aligned} \tag{10}$$

Furthermore, the energy control outer loop is performed by (11).

$$\begin{aligned} i^*_{c,z} &= -k_{p,w\Sigma}\left(w^*_{\Sigma} - w_{\Sigma} \right) - k_{i,w\Sigma}\rho_{w\Sigma} \\ \dot{\rho}_{w\Sigma} &= \left(w^*_{\Sigma} - w_{\Sigma} \right) \end{aligned} \tag{11}$$

b) Non-conventional control

Note that for the *non-conventional* control structure, the first two equations in (10) are replaced by (12), as the active current takes on the task of energy regulation.

$$\begin{aligned} i^*_{conv,d} &= -k_{p,w\Sigma}\left(w^*_{\Sigma} - w_{\Sigma} \right) - k_{i,w\Sigma}\rho_{w\Sigma} \\ \dot{\rho}_{w\Sigma} &= \left(w^*_{\Sigma} - w_{\Sigma} \right) \end{aligned} \tag{12}$$

Conversely, the circulating current is now used to regulate the power transfer of the system, calculated at the dc terminals of the converter, as shown (13).

$$\begin{aligned} i^*_{cz} &= -k_{p,pdc}\left(p^*_{dc} - p_{dc} \right) - k_{i,w\Sigma z}\rho_{pdc} \\ \dot{\rho}_{pdc} &= \left(p^*_{dc} - p_{dc} \right) \end{aligned} \tag{13}$$

4) Inner loop controllers

A phase locked loop (PLL) is used to find the angle the point of common couple (PCC) voltage vector. The rotating d-q reference frame used in the converter control has its d-axis aligned with PPC voltage vector. This definition of d-q axis allows a decoupled control of active and reactive power, where the active and reactive power at the grid connection point are given as in (14).

$$\begin{aligned} p_{ac} &= v_{pcc,d} i_{conv,d} \\ q_{ac} &= -v_{pcc,q} i_{conv,q} \end{aligned} \tag{14}$$

.

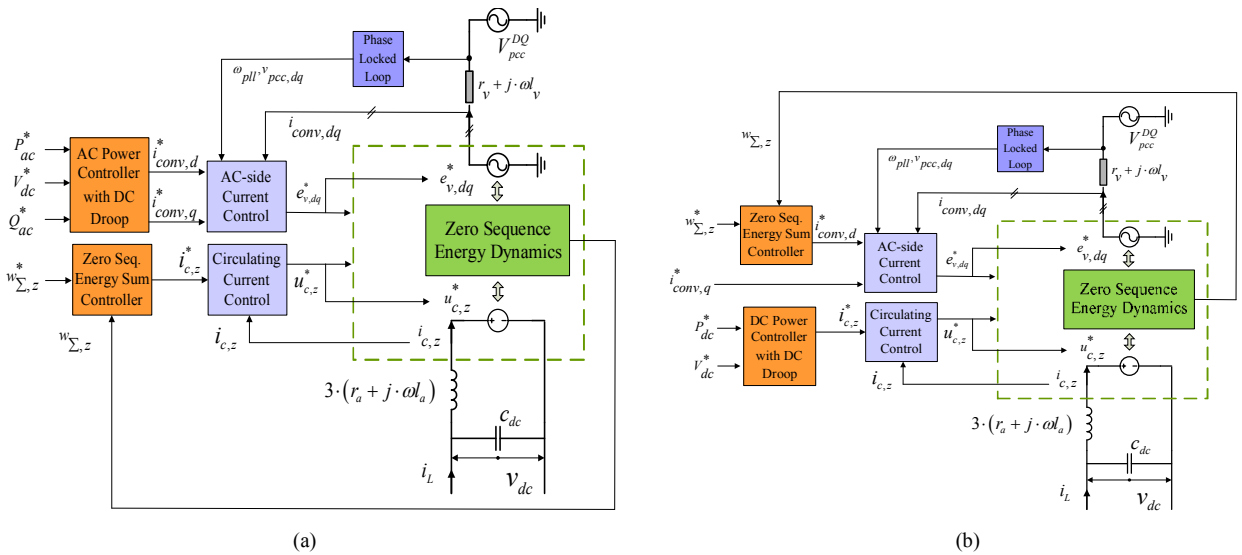

Fig. 1. Overview of assumed MMC Control Strategies with a) *conventional control:* droop controller providing the ac-side d-axis current references and b) *non-conventional control:* droop controller providing the zero-sequence circulating current reference

a) Inner controller

The inner controller regulates the current using standard PI controllers in a Synchronously Rotating d-q Reference Frame (SRRF) including decoupling feedforward terms, as indicated by (15). Furthermore, γ_d and γ_q are the states created by the integral part of the ac-grid current inner control loop whereas $k_{p,v}$ and $k_{i,v}$ are the PI proportional and integral parameters.

$$\begin{aligned} e^*_{v,d} &= k_{p,v}\left(i^*_{conv,d} - i_{conv,d}\right) + k_{i,v}\gamma_d - l_v\omega_{pll} i_{conv,q} + v_{pcc,d} \\ \dot{\gamma}_d &= i^*_{conv,d} - i_{conv,d} \\ e^*_{v,q} &= k_{p,v}\left(i^*_{conv,q} - i_{conv,q}\right) + k_{i,v}\gamma_q + l_v\omega_{pll} i_{conv,d} + v_{pcc,q} \\ \dot{\gamma}_q &= i^*_{conv,q} - i_{conv,q} \end{aligned} \tag{15}$$

5) Circulating current controller

The control of the zero-sequence of the circulating current, proportional to the dc current of the system, is calculated according to (16).

$$\begin{aligned} u^*_{cz} &= -k_{p,ucz}\left(i^*_{cz} - i_{cz}\right) - k_{i,ucz}\gamma_z \\ \dot{\gamma}_z &= \left(i^*_{cz} - i_{cz}\right) \end{aligned} \tag{16}$$

C. DC Cable Modelling

The dc cables are modelled as cascaded pi sections with parallel series branches, as proposed in [9]. The parallel branches are added to take into account the frequency dependency of the dc cable's series resistance *r* and inductance *l* per unit length.

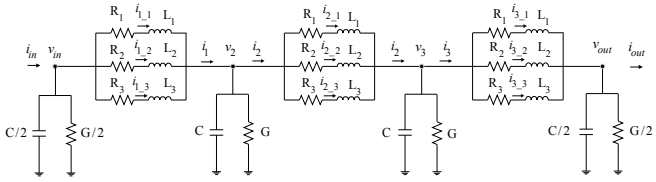

Fig. 2. Three pi section with three parallel branches cable model

Three pi-sections with three-parallel branches are used in this study as shown Fig. 2. The conductance G is ignored, and the capacitances at the beginning and end of the cable are considered in MMC converter dc side modelling as in (9).

The current in the series element of each pi-section is split amongst different parallel branches, each with its own RL dynamics. The current flowing in the j^{th} parallel branch of the k^{th} pi-section have dynamics governed according to:

$$\dot{i}_{k\_j} = \frac{1}{L_j}\left(v_k - v_{k+1} - R_j i_{k\_j}\right) \tag{17}$$

The voltage dynamics at the beginning and end of the cable are governed by:

$$\begin{aligned} \dot{v}_{in} &= \frac{2}{C}\left(i_{in} - i_1 - \frac{G}{2}v_{in}\right) \\ \dot{v}_{out} &= \frac{2}{C}\left(i_3 - i_{out} - \frac{G}{2}v_{out}\right) \end{aligned} \tag{18}$$

whereas the voltage dynamics in the middle of the cable (v_2 and v_3) are governed by:

$$\dot{v}_2 = \frac{1}{C}\left(i_1 - i_2 - G v_2\right) \tag{19}$$

D. Hybrid ac/dc system model

The complete hybrid ac/dc system model is composed of the non-linear differential and algebraic equations (DEA) listed in (1) - (19) representing different components (generator, converter and cable), and their controllers. In small signal stability studies, the DAE equations are linearized to form a linear state-space representation of the system, given by:

$$\begin{aligned} \Delta\dot{\mathbf{x}} &= \mathbf{A}\Delta\mathbf{x} + \mathbf{B}\Delta\mathbf{u} \\ \Delta\mathbf{y} &= \mathbf{C}\Delta\mathbf{x} + \mathbf{D}\Delta\mathbf{u} \end{aligned} \tag{20}$$

where **A**, **B**, **C**, and **D** are state, input, output and feed-forward matrices, respectively, and **Δx**, **Δu**, and **Δy** are state, input and output vectors, respectively. For the hybrid ac/dc power system used in this paper, the state vector **x** is:

$$\mathbf{x} = \begin{bmatrix} \mathbf{x}_{gen} & \mathbf{x}_{avr} & \mathbf{x}_{gov} & \mathbf{x}_{MMC} & \mathbf{x}_{cable} \end{bmatrix}^T \tag{21}$$

Where $\mathbf{x}_{gen}$, $\mathbf{x}_{avr}$, $\mathbf{x}_{gov}$, $\mathbf{x}_{MMC}$ and $\mathbf{x}_{cable}$ are state variables associated with generator, excitation system, governor system, MMC converter and dc cables, respectively.

$$\begin{aligned} \mathbf{x}_{gen} &= \begin{bmatrix} \delta & \Delta\omega & E_q^{'} & E_d^{'} & E_q^{''} & E_d^{''} \end{bmatrix}^T \\ \mathbf{x}_{avr} &= \begin{bmatrix} E_{fd} & x_{AVR1} & x_{AVR2} \end{bmatrix}^T \\ \mathbf{x}_{gov} &= \begin{bmatrix} x_{GOV1} & x_{GOV2} & x_{GOV3} \end{bmatrix}^T \\ \mathbf{x}_{MMC,ac} &= [i_{conv,d} \quad i_{conv,q} \quad w_{\Sigma} \quad v_{cd} \quad v_{cq} \\ &\qquad \rho_q \quad \gamma_d \quad \gamma_q \quad \kappa_{\Sigma} \quad \theta_{pll} \quad x_{pll}]^T \\ \mathbf{x}_{MMC,dc} &= \begin{bmatrix} v_{dc} & i_{c,z} & \rho_d & \xi_z \end{bmatrix}^T \\ \mathbf{x}_{cable} &= \begin{bmatrix} i_{dc1\_1} & i_{dc1\_2} & \cdots & i_{dc3\_3} & v_{dc2} & v_{dc3} \end{bmatrix}^T \end{aligned} \tag{22}$$

where θ_{pll} and x_{pll} are phase locked loop (PLL) states. Note that the MMC states are divided into ac and dc side states according to [10], such that two subsystems are defined for the converter. This separation will prove particularly useful to highlight the case were small signal interactions occur between the ac network and only the ac-side subsystem of the MMC, leaving the dc-side subsystem dynamically decoupled from the ac grid.

The input vector, **u**, for the complete hybrid ac/dc system model is made up of the references for the generator and converter controllers:

$$\mathbf{u} = \begin{bmatrix} V_{ref,i} & \omega_{ref,i} & p_{ac,i}^{*} & q_{ac,i}^{*} & v_{dc,i}^{*} & w_{\Sigma,z,i}^{*} \end{bmatrix}^T \tag{23}$$

III. INTERACTION IDENTIFICATION METHODOLOGIES

Two types of linear analysis methods were used for identification of interaction between the ac and dc parts of the hybrid ac/dc power system. The first method is based on elements of right eigenvectors or mode shapes, while the second method is based on participation factor of states in a mode. This section introduces the two interaction analyses methods used in this paper.

A. Mode shape based interaction analysis

Eigenvalues or modes of a real *nxn* state matrix **A** are *n* real or complex quantities, λ, which are roots of the characteristics equation:

$$\det(\lambda\mathbf{I} - \mathbf{A}) = 0 \tag{24}$$

For each eigenvalue λ_i, there exists an *n*-element column vector $\boldsymbol{\phi}_i$ that is a non-trivial solution of the equation:

$$\mathbf{A}\boldsymbol{\phi}_i = \lambda_i\boldsymbol{\phi}_i \tag{25}$$

$\boldsymbol{\phi}_i$ is called right eigenvector of **A** associated with the eigenvalue λ_i. Its elements indicate the relative activity of state variables when the i^{th} mode is excited. For example, the degree of activity of the sate variable x_k in the i^{th} mode is given by the magnitude of the k^{th} element of the right eigenvector, i.e. ϕ_{ki}. However, the numerical values of $|\phi_{ki}|$ depend on scaling and units selected for the associated state variables, e.g. speed in pu, angle in rad. Therefore, relative amplitudes and phases of elements of the right eigenvectors associated with similar states are used to analyze modal responses. For example, for an inter-area mode, λ_h, the elements in the right eigenvector corresponding to the speed states, $\phi_{\Delta\omega h}$, of all *n*-generators are selected to show speed mode-shape. Their relative amplitudes or mode shapes are computed as:

$$\frac{\begin{bmatrix} \left|\varphi_{\Delta\omega_1 h}\right| & \left|\varphi_{\Delta\omega_2 h}\right| & \cdots & \left|\varphi_{\Delta\omega_k h}\right| & \cdots & \left|\varphi_{\Delta\omega_n h}\right| \end{bmatrix}}{\left|\varphi_{\Delta\omega_k h}\right|}, \text{ or}$$

$$\begin{bmatrix} \dfrac{\left|\varphi_{\Delta\omega_1 h}\right|}{\left|\varphi_{\Delta\omega_k h}\right|} & \dfrac{\left|\varphi_{\Delta\omega_2 h}\right|}{\left|\varphi_{\Delta\omega_k h}\right|} & \cdots & 1 & \cdots & \dfrac{\left|\varphi_{\Delta\omega_n h}\right|}{\left|\varphi_{\Delta\omega_k h}\right|} \end{bmatrix} \tag{26}$$

where $\phi_{\Delta\omega_k h}$ is the speed state associated element with the largest magnitude. A large relative amplitude in (26) implies significant "involvement" of the state in mode λ_h [11]. The relative phase between the mode shapes indicates how the machines swing in relative to each other.

In this paper, modes shapes of electromechanical modes are used to study interaction between asynchronous grids

connected through an MMC based MTDC grid for two types converter control structures.

B. Participation factor based interaction analysis

This interaction mode identification method is proposed by [12]. With this method, the hybrid ac/dc system is divided into subsystems. Each subsystem represents either an ac grid, a converter or a dc grid, and is formed by grouping the appropriate state variables. For example, all states of generator, AVR and governor, listed in (22), make up an ac grid subsystem.

A parameter $\eta_{\alpha i}$ is defined in [12] as a measure of the cumulative participation of subsystem α in mode i. Mathematically, $\eta_{\alpha i}$ is defined as the ratio of L_1-norm of the vector of participation factors of states in subsystem α in mode i ($p_{\alpha,i}$) to the L_1-norm of the vector of participation factors of all states in mode i (p_i).

$$\eta_{\alpha i} = \frac{\|p_{\alpha i}\|}{\|p_i\|} \tag{27}$$

Modes in which more than one subsystem participate in are classified as interaction modes. For threshold value of χ, an interaction mode j is a mode where $\eta_{\alpha j} > \chi$ for two or more subsystems.

IV. Study System Configuration and Analysis

The study system is three terminal MMC based MTDC grid connecting three asynchronous ac grids; see Fig. 3. All three ac grids contain multiple generators, and represent large power systems. System topology and data for Grid#1, Grid#2, and Grid#3 are taken from benchmark systems given in [13], [14], and [15], respectively. The dc grid is a symmetrical monopolar system with ±200 kV voltage rating.

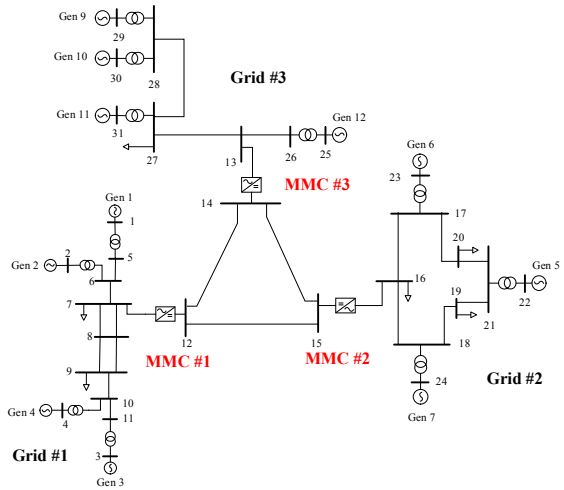

Fig. 3. Hybrid ac/dc test study system

The hybrid ac-dc study system is modelled in Matlab/Simulink by combining the differential and algebraic equations (DEA) representing the different power system elements and their controllers; presented in Section II. The dc grid is operated in dc voltage droop control mode with droop constant of 4%. All converters are set to constant reactive power control with zero reference. Two cases of MMC converter control structures were studied. In the first case, Case 1, conventional type of MMC control structures is used (Fig. 1. (a)), while in Case 2 a non-conventional type of control structure is used (Fig. 1. (b)).

The linearized state space representation of the system is computed by using the linearization feature of Matlab/Simulink. The system has in total 183 number of modes. TABLE I. lists poorly damped eigenvalues of the study system with damping ratio less than 10%.

TABLE I. MODES WITH DAMPING RATIO LESS THAN 10%

Eigenvalue	f [Hz]	ζ [%]	Dominant States Variables
$\lambda_{130,131} = -0.05 \pm j2.92$	0.46	1.56	$\Delta\omega_3, \Delta\omega_4, \delta_1, \delta_2, \Delta\omega_1$
$\lambda_{128,129} = -0.13 \pm j3.4$	0.54	3.78	$\delta_{11}, \Delta\omega_{12}, \Delta\omega_{10}, \omega_9, E'_{q12}$
$\lambda_{121,122} = -0.48 \pm j6.08$	0.97	7.83	$\delta_{10}, \Delta\omega_{11}, \Delta\omega_{10}, \Delta\omega_9, E''_{q11}$
$\lambda_{113,114} = -0.69 \pm j7.55$	1.20	9.04	$\delta_5, \Delta\omega_6, \Delta\omega_7, \delta_6, E''_{d6}$
$\lambda_{115,116} = -0.64 \pm j6.85$	1.09	9.30	$\delta_3, \Delta\omega_4, \Delta\omega_3, \delta_2, \delta_1$
$\lambda_{119,120} = -0.68 \pm j7.18$	1.14	9.42	$\delta_9, \Delta\omega_9, \Delta\omega_{10}, E''_{d10}, E''_{d9}$

All of the poorly damped modes are electromechanical modes involving the rotor angle and speed deviation states of the generators in the different ac grids. From the frequency of the modes and the dominating states, it can be observed that $\lambda_{130,131}$ and $\lambda_{128,129}$ are interarea modes representing oscillations of groups of generators in different areas Grid 1 and Grid 3, respectively, while $\lambda_{121,122}$, $\lambda_{113,114}$, $\lambda_{115,116}$ and $\lambda_{119,120}$ are local (intra-area) modes.

A. Observability based method

TABLE II. lists mode shapes of the two poorly damped inter-area modes for speed state variables. The values are normalized based on the highest mode shape magnitude for the speed state variables.

TABLE II. MODE SHAPES OF INTER-AREA MODES IN GRID 1 AND GRID 3 FOR SPEED STATE VARIABLES

States	*Case 1 (Conventional)*		*Case 2 (Non-Conventional)*	
	$\lambda_{130,131}$	$\lambda_{128,129}$	$\lambda_{130,131}$	$\lambda_{128,129}$
	-0.05 ± j 2.92	***-0.13 ± j 3.4***	***-0.05 ± j 2.92***	***-0.13 ± j 3.4***
$\Delta\omega_1$	0.347	0	0.347	0
$\Delta\omega_2$	0.374	0	0.374	0
$\Delta\omega_3$	1	0.001	1	0
$\Delta\omega_4$	0.936	0.001	0.936	0
$\Delta\omega_5$	0.002	0	0	0
$\Delta\omega_6$	0.002	0	0	0
$\Delta\omega_7$	0.002	0	0	0
$\Delta\omega_8$	0.002	0.765	0	0.766
$\Delta\omega_9$	0.002	0.786	0	0.788
$\Delta\omega_{10}$	0.002	0.476	0	0.477
$\Delta\omega_{11}$	0.001	1	0	1

It is clear that speed states in a grid where a mode dominates have high mode shape magnitudes or high involvement in the mode, e.g. $\lambda_{130,131}$ has high observability in speed states in Grid 1 and $\lambda_{128,129}$ has high observability in speed states in Grid 3. However, these modes are also observable, to a small extent, in the other grids. Mode $\lambda_{130,131}$ has 0.2% observability in almost all generators that are found in grids other than where it dominates, i.e. Grid 2 and 3, while mode $\lambda_{128,129}$ has 0.1% observability in Generators that are found in Grid 1. However small, observability of a mode that is dominant in a grid that are asynchronously connected through an MTDC grid indicates an ac-ac interaction. On the other hand, when the non-conventional control structure is used, the poorly damped modes are only observable in the grid where they are dominating and they are not observable in the speed state of the other grids. This implies that the non-conventional converter control structure removes the ac-ac interactions observed in the case with conventional control structure.

B. Participation factor based method

In this analysis method, the hybrid ac/dc grid is divided into 10 subsystems: three subsystems each made up of ac grid states, three subsystems each made up of PLL and MMC ac side states, three subsystems each made up of MMC dc side states, and one sub system made up of the (three) dc cables. Interaction between the subsystems are studied using the participation factor method described in Section III.B for a threshold value of χ =10%.

TABLE III. compares the total number of interaction modes between different number of subsystems for two cases of MMC converter control modes. The cumulative participation (η) of each subsystem is at least 10%.

TABLE III. TOTAL NUMBER OF INTERACTION MODES BETWEEN DIFFERENT NUMBER OF SUBSYSTEMS

Number of subsystems	**Case1 (Conventional)**	**Case 2 (Non-conventional)**
2	31	20
3	13	7
4	4	1

Most of the interaction modes are between two or three subsystems. There are no modes with participation from more than four subsystems. When comparing Case 1 and 2, it can be seen that there are a higher number of interaction modes when conventional control structure is implemented than the non-conventional case. TABLE III. only shows how many interaction modes exist and how many subsystems participate, but does not indicate which subsystems are participating in the modes. In the following analyses, interaction modes are studied further focusing on ac-dc subsystem and converter subsystems interactions.

1) AC-DC interaction modes

Fig. 4. and Fig. 5. show interaction modes with at least 10% cumulative participation from Grid#2 and MMC#2 (either ac side or dc side subsystem) with conventional and non-conventional MMC control structures, respectively. In Fig. 4. , mainly Grid#2 and MMC#2 ac side subsystems participate in all interaction modes. In addtion, there is different level of participation from MMC#2 dc side subsystem in all interaction modes except λ_{104}.

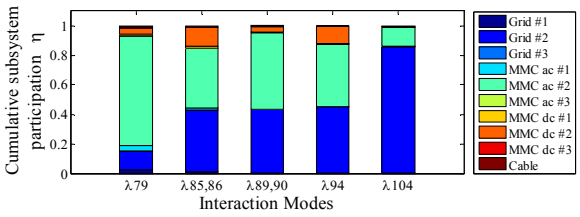

Fig. 4. Interaction modes between Grid #2 and MMC #2 subsystems with convensional MMC control structure

In Fig. 5. , the interaction modes identified between ac and dc subsystems have participation only from Grid#2 and ac side MMC#2 subsystems. This shows that under the non-conventional MMC control structure, only the ac grid and the ac-side subsystem of the converter interact, and there is no interaction between the ac grid subsystem and the converter's dc side subsystem.

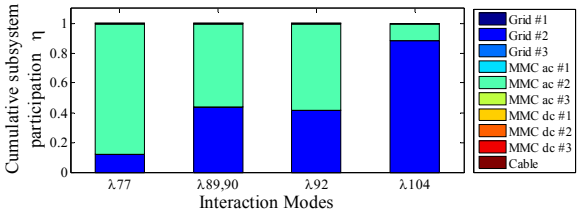

Fig. 5. Interaction modes between Grid #2 and MMC #2 subsystems with non-convensional MMC control structure

Similar results were found for interaction modes between Grid #1 and MMC#1, and between Grid #3 and MMC#3. The results are not presented here due to lack of space.

2) Converter interaction modes

Fig. 6. shows converter interaction modes with 10% cumulative participation from all three MMC converters for the conventional converter control structure. In modes $\lambda_{45,46}$ and $\lambda_{47,48}$, cable subsystem participate in addition to the MMC subsystems, while in λ_{182} and λ_{183}, only converter ac-side subsystems participate.

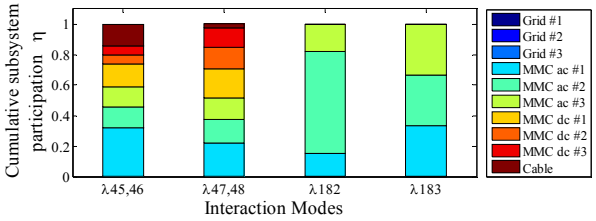

Fig. 6. Interaction modes with participation from all converters under conventional converter cotnrol

Interaction modes for non-conventional type of converter control mode are shown in Fig. 7. The participating subsystems are from all three converters, but the dc side subsystems of the converters. Unlike Fig. 6. the ac side converter subsystem do not participate. The interaction is limited to dc cable and/or dc side converter subsystems.

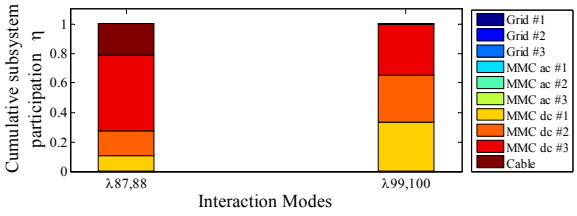

Fig. 7. Interaction modes with participation from all converters for non-conventional converter control

V. CONCLUSION

This paper analyzed and compared interaction between ac and dc grids in a hybrid ac/dc power system for two types of MMC converter control structures. It used linear analysis methods, which are based mode shapes and participation factors for the analysis. It was shown using mode shapes of poorly damped inter-area modes for generator speed state that there exists weak coupling between asynchronous grids linked via MTDC when MMCs are control using conventional converter controller. In contrast, when the non-conventional type of control structure is used on the MMCs, there is no dynamic coupling between the asynchronous ac grids. Results from the participation factor based analysis showed that the non-conventional type of control structures decouple the ac and dc side of the converter and that converter interactions are limited to the dc side only without involving the ac side of the converter. In general, this paper showed that the non-conventional MMC converter structure decouples the ac and dc side of the MMC converter, thus avoiding interaction between the ac and dc grids.

REFERENCES

[1] A. Lesnicar and R. Marquardt, "An Innovative Modular Multilevel Converter Topology Suitable for a Wide Power Range," in *Power Tech Conference Proceedings, 2003 IEEE Bologna*, 2003, p. 6 pp. Vol.3.

[2] G. Bergna, J. A. Suul, and S. D. Arco, "State-Space Modelling of Modular Multilevel Converters for Constant Variables in Steady-State," in *2016 IEEE 17th Workshop on Control and Modeling for Power Electronics (COMPEL)*, 2016, pp. 1-9.

[3] A. a. J. Far and D. Jovcic, "Circulating Current Suppression Control Dynamics and Impact on Mmc Converter Dynamics," in *2015 IEEE Eindhoven PowerTech*, 2015, pp. 1-6.

[4] A. Jamshidifar and D. Jovcic, "Small-Signal Dynamic DQ Model of Modular Multilevel Converter for System Studies," *IEEE Transactions on Power Delivery,* vol. 31, pp. 191-199, 2016.

[5] V. Najmi, M. N. Nazir, and R. Burgos, "A New Modeling Approach for Modular Multilevel Converter (Mmc) in D-Q Frame," in *2015 IEEE Applied Power Electronics Conference and Exposition (APEC)*, 2015, pp. 2710-2717.

[6] G. Bergna-Diaz, J. A. Suul, and S. D. Arco, "Small-Signal State-Space Modeling of Modular Multilevel Converters for System Stability Analysis," in *2015 IEEE Energy Conversion Congress and Exposition (ECCE)*, 2015, pp. 5822-5829.

[7] J. Freytes, L. Papangelis, H. Saad, P. Rault, T. V. Cutsem, and X. Guillaud, "On the Modeling of Mmc for Use in Large Scale Dynamic Simulations," in *2016 Power Systems Computation Conference (PSCC)*, 2016, pp. 1-7.

[8] J. Machowski, J. Bialek, and J. Bumby, *Power System Dynamics: Stability and Control*: WILEY, 2008.

[9] J. Beerten, G. Bergna-Diaz, S. D' Arco, and J. A. Suul, "Comparison of Small-Signal Dynamics in Mmc and Two-Level VSC HVDC Transmission Schemes," in *ENERGYCON*, ed. Leuven, Belgium, 2016.

[10] G. Bergna-Diaz, J. A. Suul, and S. D' Arco, "Impact on Small-Signal Dynamics of Using Circulating Currents Instead of AC-Currents to Control the DC Voltage in Mmc HVDC Terminals," in *IEEE Energy Conversion Congress & Expo (ECCE)*, Milwaukee, USA, 2016.

[11] M. J. Gibbard, P. Pourveik, and D. J. Vowles, *Small-Signal Stability, Control and Dynamic Performance of Power Systems*. Adelaide: University of Adelaide Press, 2015.

[12] J. Beerten, S. D. Arco, and J. A. Suul, "Identification and Small-Signal Analysis of Interaction Modes in VSC MTDC Systems," *IEEE Transactions on Power Delivery,* vol. 31, pp. 888-897, 2016.

[13] P. Kundur, *Power System Stability and Control*: McGraw-Hill Inc., 1994.

[14] P. M. Anderson and A. A. Fouad, *Power System Control and Stability*: IEEE Press, 1993.

[15] C. Canizares, T. Fernandes, E. G. Junior, G. L. Luc, M. Gibbard, I. Hiskens, *et al.*, "Benchmark Models for the Analysis and Control of Small-Signal Oscillatory Dynamics in Power Systems," *IEEE Transactions on Power Systems,* vol. PP, pp. 1-1, 2016.